Available online at www.sciencedirect.com
ScienceDirect
Ceramics International 36 (2010) 1971–1976
CERAMICS INTERNATIONAL
www.elsevier.com/locate/ceramint

Evaluation and comparison of the microstructure and mechanical properties of fibrous Al_2O_3–(m-ZrO_2)/t-ZrO_2 composites after multiple extrusion steps

Swapan Kumar Sarkar, Byong Taek Lee *

Department of Biomedical Engineering and Materials, Soonchunhyang University, 366-1 Ssangyoun-dong, Cheonan City, Chungnam 330-090, South Korea

Received 11 January 2010; received in revised form 10 March 2010; accepted 20 April 2010
Available online 9 June 2010

Abstract

Microstructural variations in the Al_2O_3–(monoclinic-ZrO_2)/tetragonal-ZrO_2 core/shell composites (Al_2O_3–(m-ZrO_2)/t-ZrO_2) were tailored using different volume fractions of the core and shell by the multi-pass co-extrusion process. To introduce continuously fibrous microtextures with varying dimensions of microstructure, various volume fractions of the Al_2O_3–(m-ZrO_2) core and t-ZrO_2 shell phases were used (40/60, 50/50 and 60/40). The effect of the number of extrusion passes on the control of microstructure and the corresponding composite's mechanical properties were investigated. The bending strength and fracture toughness values were shown to increase as the t-ZrO_2 shell volume fraction increased, which was unlike the Vickers hardness value. However, the fracture toughness value was higher for 4th pass composites compared to 5th pass composites due to the presence of the fibrous core/shell microstructure. In addition, the bending strength was higher for 5th pass composites. Detailed microstructural analysis was carried out by SEM.

Keywords: A. Extrusion; B. Microstructure-final; D. Al_2O_3; ZrO_2

1. Introduction

Al_2O_3 ceramics can be used in many applications that require severe operating conditions like very high temperature, excessive corrosive environment and very low wear [1]. The excellent thermal and chemical stability of this ceramic together with its very high hardness value allows this material to perform well under these harsh conditions. However, like other ceramics, this ceramic has low fracture toughness and can barely sustain any impact load. The brittleness of this material limits its application despite its other excellent features. For decades researchers have been trying to improve the mechanical properties of Al_2O_3 based ceramics. Some of these attempts have included the incorporation of whiskers or particles [2–4], the addition of metal by electroless deposition or milling, etc. [5,6]. It has been reported that whisker and fiber reinforced ceramic matrix composites displayed remarkable fracture toughening due to crack bridging and fibrous pull-out mechanisms. However, fabrication difficulties and cost considerations have prevented widespread use of this method [7]. Another important approach that was developed was designing the microstructure by exploiting specific materials properties such as the phase transformation phenomena of t-ZrO_2, or by designing specific structural features with lamellar or fibrous microstructures [8–10].

Among the methods to improve the materials properties of Al_2O_3 based ceramics, the development of the laminated microstructure using the ZrO_2 phase has been specifically popular and extensively investigated due to its ease and low cost fabrication [9,11]. However, fine scale microstructure modifications in the laminate are difficult. Recently, an interesting approach based on macroscaled microstructure control using the multi-pass extrusion process was developed and has been shown to be an effective way to design and control fine scale microstructure with different ceramics [12–14]. This method has been used to fabricate Al_2O_3 based ceramics with different microstructures and it was shown that this method allows for very fine control over the resulting microstructure. In previous

* Corresponding author. Tel.: +82 41 5702427; fax: +82 5772415.
E-mail address: lbt@sch.ac.kr (B.T. Lee).

0272-8842/$36.00
doi:10.1016/j.ceramint.2010.05.011

studies, well controlled and homogeneous Al_2O_3–(m-ZrO_2)/t-ZrO_2 fibrous composites with a core/shell microstructure were fabricated and the resulting microstructure was found to be depended on the relative composition of the core and shell [14,15]. The fracture toughness was increased due to toughening mechanisms, such as microcracks and phase transformation of the t-ZrO_2. The extrusion pass number was found to be a crucial parameter for microstructural refinement and, to some degree, this parameter was also important to the mechanical performance of the composites. However, a detailed investigation on the dependence of the extrusion pass number with varying compositions of the constituent phases of the fibrous core/shell microstructure was not conducted.

In this work, fibrous Al_2O_3–(m-ZrO_2)/t-ZrO_2 composites with different core/shell volume fractions were fabricated using the multi-pass extrusion process. The effect of the extrusion pass number on the resulting microstructure was investigated as a continuation of our previous work. Variations in the materials properties of the composites with each pass at different core/shell volume fractions were also investigated.

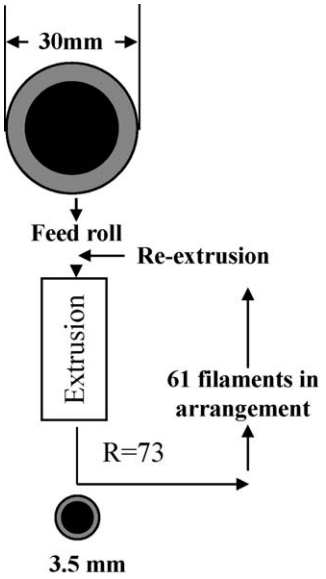

Fig. 1. Schematic diagram of the extrusion process for fabricating the fibrous core/shell composites.

2. Experimental procedure

The extrusion process was carried out by mixing the ceramic powder with an organic binder to make an extrudable plastic material; they were then formed by warm pressing to create a feed roll of preferential geometry and then repeated extrusions were carried out using the successive filaments after grouping them into a bundle of 61 filaments. The starting Al_2O_3 powder (AKP-50, Sumimoto, Japan), monoclinic ZrO_2 (TZ-0Y, Tosoh, Japan) and tetragonal ZrO_2 powders (TZ-3Y, Tosoh, Japan) had an average particle size of about 300, 80 and 80 nm, respectively. The Al_2O_3–(25% m-ZrO_2) powders were mixed by ball milling for 24 h in ethanol. The mixtures of Al_2O_3–(m-ZrO_2) powders and tetragonal Zirconia (t-ZrO_2) powder were blended separately with a polymer binder using a heated blender (Shina Platec. Co., Suwon, South Korea) at a temperature of 120 °C. Ethylene Vinyl Acetate (EVA) (Elvax 250 and Elvax 210, Dupont, USA) polymers were used as binders of the ceramic powders. For lubrication purposes, stearic acid ($CH_3(CH_2)_{16}COOH$, Daejung Chemicals & Metals Co. Ltd., Korea) was added. Mixtures of Al_2O_3–(m-ZrO_2)/polymer (depicted as AP) were extruded as a cylindrical rod and the ZrO_2/polymer (depicted as ZP) was compacted into the shell shape by warm pressing. After combining them, they were made into a feed roll 30 mm in diameter with the AP in the core and ZP in the shell. Different volume fractions of the core/shell were made by changing the core diameter and shell thickness. Fig. 1 shows the schematic diagram of the extrusion process. The core/shell design of the Al_2O_3–(m-ZrO_2)/t-ZrO_2 green composites is shown above, which was the primary unit of the microstructure. The grey outer contrast is for the t-ZrO_2 shell and the inner black circle is for the Al_2O_3–(m-ZrO_2) core. The outer diameter of the feed roll was set to 30 mm and the core/shell volume fractions were varied to 40/60, 50/50 and 60/40 (vol%).

The feed roll was mounted on a heated extrusion die and then extruded at an extrusion ratio of approximately 73:1. The shell thickness and core diameter of the individual composites were made with a specially designed die and the volume fractions were of the green preforms only. So the volume fractions stated in this manuscript represent that of the green composites.

The feed roll for each composition was extruded to obtain the 1st passed filaments, which were 3.5 mm in diameter. The 1st passed filaments were arranged in the same die and extruded again to obtain the 2nd passed filaments that were also 3.5 mm in diameter. The process was repeated until the 5th passed filaments were obtained. The extrusion temperature and rate were 120 °C and 8 mm/min, respectively. The binder was removed from the green body during the binder burning-out process, which was carried out at 700 °C under a flowing nitrogen atmosphere. The samples were then sintered at 1450 °C for 2 h in air. The density of the sintered bodies was measured using the Archimedes Method. The hardness of the sintered bodies was measured using the Vickers Hardness Tester (HV-112, Akashi, Yokohama, Japan) under a load of 1 kg for 10 s. To investigate the fracture toughness K_{1C}, it was measured by the indentation method using Evan's equation:

$$K_{IC} = 0.16\,H\,a^{1/2}\left(\frac{c}{a}\right)^{-3/2}$$

where H = Vickers hardness, a = half of indentation diagonal, c = half of the crack length from the indentation center.

In order to measure the bending strength, four point bending test was carried out using a Universal Testing Machine (Unitech^{TM}, R&B, Korea). The bend bars were cut 30 mm in length and were 2.65 mm in diameter. No surface preparation was made because the sintered specimens had smooth surfaces and were cylinder shaped. Microstructural variations of the fibrous composites at different volume fractions were examined

using a Field Emission Scanning Electron Microscope (FE-SEM, JSM 6335F, JEOL, Tokyo, Japan).

3. Results and discussion

SEM images of the 4th passed core/shell microstructure of the composites with different volume fractions are shown in Fig. 2. Fig. 2(a)–(c) shows the 4th passed sintered composites with core/shell composition of 40/60, 50/50 and 60/40, respectively. The core/shell microstructure was clearly observed and the distribution of the microstructural features was uniform in each case. However, as shown in Fig. 2(d)–(f), in the 5th pass composites at the same 40/60, 50/50 and 60/40 core/shell compositions, the characteristic core/shell features could no longer be identified. The two-dimensional reduction ratio of 61:1 from the 4th pass to 5th pass was high enough to distort the core/shell microstructure after the 5th extrusion. The miniaturization of the microstructure during extrusion obeys the following equation:

$$D_{n+1} = \frac{D_0}{R^{n/2}}$$

where D_{n+1} = dimension of the nth pass filament, D_0 = dimension of the feed role and R = reduction ratio.

For the 50/50 composites with a feed role Al_2O_3–(m-ZrO_2) core diameter of 22 mm, the same core after the 5th pass should theoretically become approximately 750 nm. But in practice the actual dimension is lower than this due to the repeated viscous flow of the plastic ceramic + polymer. As a result, the core diameter in the 5th pass was expected to be less than 750 nm. However, the particle size of Al_2O_3 was found to be 300 nm and due to the closeness in dimension, the core phase was not distinct from the shell phase and consequently the phase could not be identified as a continuous fiber and was mixed with the t-ZrO_2 phase. Thus, it was impossible to control the microstructure under these conditions. During sintering, the grain growth of Al_2O_3 was also significant and at 1450 °C the grain size after growth was greater than the diameter of the core. This also prohibits the existence of the core as a continuous fiber in the dimensional vicinity of the core fiber. The network type microstructure with t-ZrO_2 was completely disrupted and a random microstructure like that of a duplex composites made by mechanical mixing of the powder was produced. Nevertheless, the microstructure showed a homogenous distribution of the Al_2O_3–(m-ZrO_2) phase within the tZrO_2 matrix. However, changes in the geometry of the green body as a function of the number of extrusion passes were reported in the work of [13]. However, from this experiment, it was apparent that the microstructure of the composites could no longer be controlled and the characteristic core/shell microstructure could not be retained when the number of repeated extrusions was greater than 4. Obviously, fine fibrous microstructures could be produced if the particle size was much smaller than the one used in this study. Control over the development of microstructural textures and dimensions depends on several factors such as the initial feed role diameter, reduction ratio in corresponding extrusions (i.e., the geometry of extrusion die) and the particle size of the starting powders.

Fig. 3 shows longitudinal section SEM images of the Al_2O_3–(m-ZrO_2)/t-ZrO_2 composites fabricated with (a and d) 40/60, (b and e) 50/50 and (c and f) 60/40 core/shell volume fractions. In the low magnification images of the 4th pass composites (a–c), continuous fibers were clearly observed. The fibrous monoliths of the core and shell phases were prolonged through the entire length. The uni-directional alignment of the fibrous monoliths was well maintained, resulting in the formation of a homogeneous microstructure. The shell thickness gradually decreased as the volume fraction of the shell decreased. The average values of t-ZrO_2 shell thickness and the Al_2O_3–(m-ZrO_2) core diameter for all the composites were shown in Table 1. However, at further extrusion passes the fibrous microstructure was barely identified, as shown in Fig. 3(d)–(f). Under these conditions, it looked more like a random mixture if not carefully observed. The fibrous microstructure was only

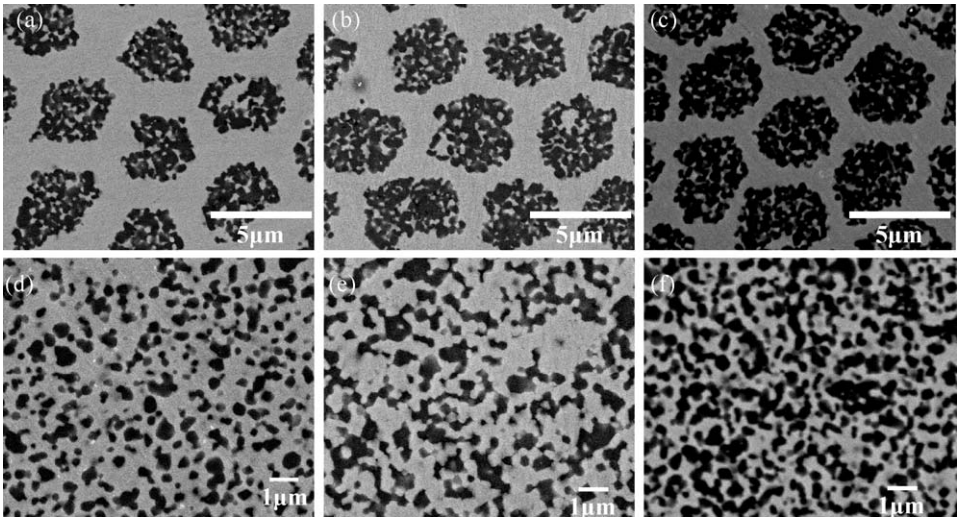

Fig. 2. SEM images of the cross-section of the 4th pass extruded body: (a) 40:60, (b) 50:50 and (c) 60:40 core/shell volume fractions. SEM images of the cross-section of the 5th pass extruded body: (d) 40:60, (e) 50:50 and (f) 60:40 core/shell volume fractions.

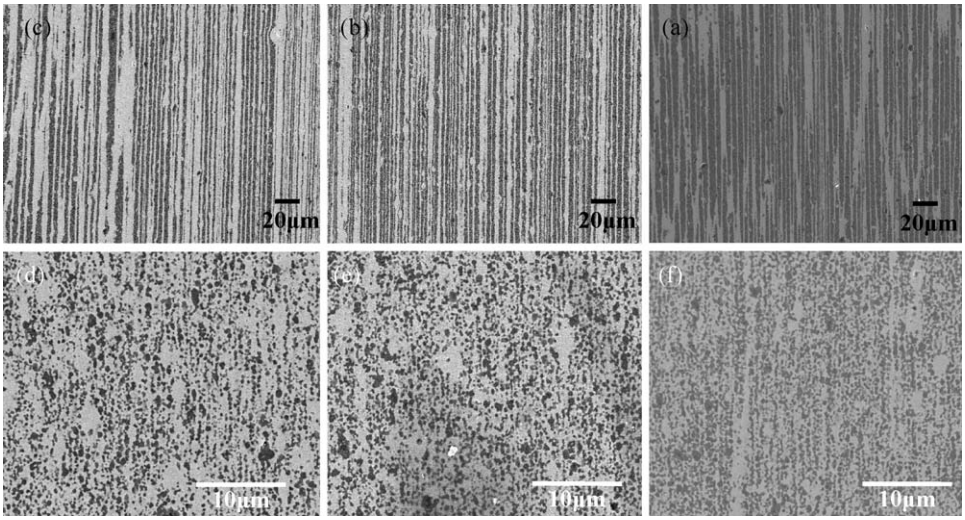

Fig. 3. SEM images of the 4th pass longitudinal section for different core/shell volume fractions: (a) 40:60, (b) 50:50 and (c) 60:40. SEM images of the longitudinal section of the 5th pass extruded body: (d) 40:60, (e) 50:50 and (f) 60:40 core/shell volume fractions.

Table 1
Microstructural dimension of the composites.

Composition	40/60	50/50	60/40
Core diameter (μm)	3.3	3.6	3.8
Shell thickness (μm)	1.8	1.3	1.0

slightly noticeable in Fig. 3(f) at the highest core phase at the 60/40 core/shell composition. As shown in Fig. 4, the microstructure was clearly visible in the enlarged longitudinal sectional SEM images. A relative change in microstructure as a function of volumetric composition was observed in the 4th pass composites (a–c), whereas in the 5th pass composites (Fig. 4(d)–(f)) the fibrous microstructural feature faded away.

This was because the rheological property of the core and shell was not exactly the same and the slight mismatch resulted in a difference in the linear flow behavior of the core and shell materials. In the reduction cone of the extrusion die, the infinitesimal relative movement of the core and shell phase significantly disturbed the microstructure as the microstructure itself was becoming very fine, near the sub-micrometer dimension range. To obtain the successive passed filaments in every extrusion pass, a pre-compaction step was carried out. This caused a lateral flow of the green material, which covered the gaps in between the individual cylindrical filaments and resulted in slight deformation [15]. This lateral flow of material may have caused the irregular core geometry, although it was perfectly round in the 1st pass green composites. Based on this observation, we believe that using an optimum die design and subsequent pre-filling of the gaps among filaments will eliminate the lateral material flow during pre-extrusion compaction and may make the microstructure more uniform up to the 5th pass. Of course, the particle size is the most important parameter in determining the dimension of the microstructure and hence the pass number.

The relative density, Vickers hardness, bending strength and fracture toughness of the composites were shown in Table 2. To

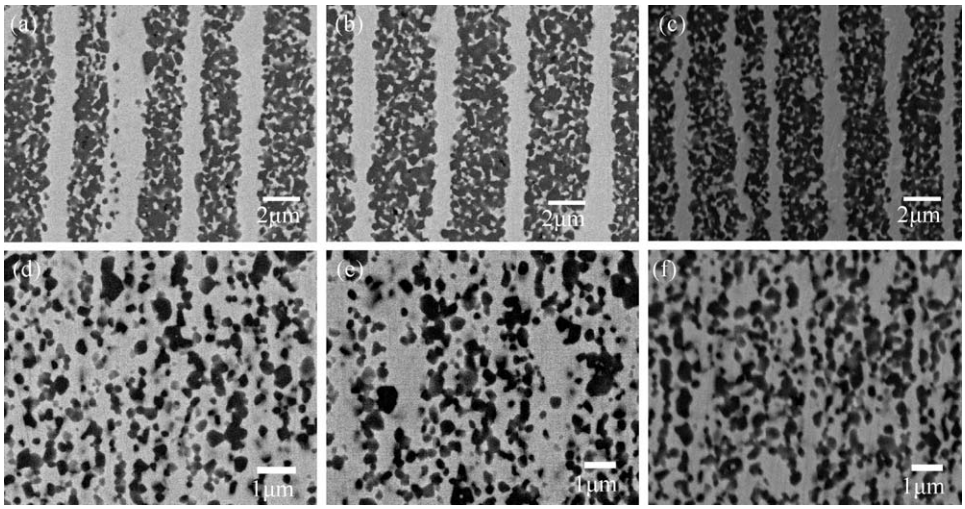

Fig. 4. SEM images of the 4th pass longitudinal section for different core/shell volume fractions: (a) 40:60, (b) 50:50 and (c) 60:40. SEM images of the longitudinal section of the 5th pass extruded body: (a) 40:60, (b) 50:50 and (c) 60:40 core/shell volume fractions.

Table 2
Material properties of the composites.

	Property							
	Relative density		Vickers hardness		Bending strength		Fracture toughness	
	4th pass	5th pass	4th pass	5th pass	4th pass	5th pass	4th pass	5th pass
Composition								
40/60	97.66	97.885	1388	1408	941.7	915	7.36	7.260
50/50	98.47	98.628	1409	1431	912.9	1082	6.867	7.156
60/40	98.91	98.91	1447	1478	874.8	1121	6.683	6.983

calculate the relative density, the initial volume fractions of the constituent phases tailored in the green ceramic was also used in the case of the sintered ceramic. In both 4th pass and 5th pass composites, the relative density slightly increased as the core phase increased. The Vickers hardness also increased as the core phase increased for both 4th and 5th pass composites. However, in the case of the 5th pass composites, the hardness value was higher than that of the 4th pass composites. The highest value for 4th pass and 5th pass composites were 1447 and 1478 Hv, respectively. The bending strength value displayed the exact opposite trend for the 4th pass and 5th pass composites as a function of volume fraction. For the 40/60 core/shell composites, the bending strength values were comparable for the 4th and 5th pass composites. But as the core phase composition increased in the 4th pass composites, the bending strength value gradually decreased, whereas in the 5th pass composites, it rapidly increased with the highest value of 1121 MPa for the 60/40 core/shell composites. This was mainly due to the presence of the defined and well developed fibrous microstructure in the 4th pass composites, where an increased volume fraction of the lower bending strength Al_2O_3 phase, which was unmixed with the t-ZrO_2 phase, independently contributed to this property. On the other hand, in the 5th pass composites, the Al_2O_3 and ZrO_2 phases were almost completely mixed with each other and the bending strength value was that of a homogeneously mixed composite, which was higher compared to both monolithic Al_2O_3 and t-ZrO_2. This demonstrates the role of the fibrous microstructure on the bending strength value of the composites. However, the bending strength value was considerably higher than the value obtained by conventional powder metallurgy processes [16]. The higher bending strength was achieved probably because of the unique processing route and lack of large structural flaws and processing defects. The role of residual stress might have an effect since the thermal expansion coefficient (CTE) of Al_2O_3 and ZrO_2 phases was different and after sintering of residual stress was developed inside the composites. It was established that the incorporation of m-ZrO2 within the AlO_3 phase can create microcracks at the phase boundary, which in effect can decrease the bending strength [8].

The fracture toughness value decreased as the Al_2O_3 rich core phase was increased for both 4th and 5th pass composites. This result was expected since the t-ZrO_2 rich phase contributes to the fracture toughness through the tetragonal to monoclinic phase transformation. However, in the 4th pass composites, the fracture toughness was higher for 40/60 core/shell composites compared to that of the 5th pass composites. In the 60/40 composites the value of fracture toughness in the transverse plane was lower compared to that of the 5th pass. Clearly the change in microstructure affected the fracture toughness, although this effect was not significant. The fracture toughness value was measured by the indentation method, which has been reported to give only an indication of the approximate trend of fracture toughness instead of the original value. However, a relative comparison of the fracture toughness of the composite systems using the same indentation load can be fairly accurate in assessing the trends in variation. From this observation, we could conclude that the core/shell microstructure affected the fracture toughness value and improved it slightly, although it had a negative effect on the bending strength value.

In this work, the fibrous monolithic Al_2O_3–(m-ZrO_2)/t-ZrO_2 ceramics with a core/shell microstructure were developed with different core and shell volume fractions and the microstructures were characterized in relation to the pass number of extrusions. Under the experiment condition used in this study, the retention of core/shell microstructure was possible up to the 4th pass of extrusion. Although the microstructure was significantly deformed compared to the initial regular core/shell geometry, the fibrous microstructure was still present. However, a subsequent pass completely disrupted the fibrous microstructure. The material properties of both 4th pass and 5th pass composites were evaluated for ceramics fabricated with different volume fractions. In these experiments, the bending strength values were higher for the 5th pass composites, whereas the fracture toughness value was higher for the 4th pass composites when the relative composition of the t-ZrO_2 phase was higher.

4. Conclusion

Fibrous Al_2O_3–(m-ZrO_2)/t-ZrO_2 composites with different core/shell volume fractions (40/60, 50/50 and 60/40) were fabricated using the multi-pass extrusion process. The dependence of the material properties on the volume fractions in relation to the extrusion pass no. was investigated. The microstructure was successfully controlled both in the transverse and longitudinal directions up to the 4th passed filaments. However, control over the microstructure could not be achieved in case of the 5th pass composites irrespective of the core/shell composition. The mechanical properties were

evaluated for all the compositions at different pass numbers. Vickers hardness decreased with an increase in the shell volume fraction, i.e., of the ZrO_2 phase, whereas the bending strength and fracture toughness increased. The 5th pass composites fracture toughness was slightly decreased compared to the 4th pass, although the bending strength increased. This demonstrated the effect of the core/shell fibrous microstructure on the mechanical properties of the fabricated composites.

References

[1] B.T. Lee, A. Nishiyama, K. Hiraga, Micro-indentation fracture behavior of Al_2O_3–24 vol%$ZrO_2(Y_2O_3)$ composites studied by transmission electron microscopy, Materials Transaction 34 (1993) 682–686.

[2] Y. Fu, Y.W. Gu, H. Du, SiC whisker toughened Al_2O_3–(Ti, W)C ceramic matrix composites, Scripta Materialia 44 (2001) 111–116.

[3] P. Pettersson, M. Johnsson, Thermal shock properties of alumina reinforced with Ti(C,N) whiskers, Journal of European Ceramic Society 23 (2003) 309–313.

[4] B.K. Jang, Microstructure of nano SiC dispersed Al_2O_3–ZrO_2 composites, Material Chemistry and Physics 93 (2005) 337–341.

[5] I.H. Oh, J.Y. Lee, J.K. Han, H.J. Lee, B.T. Lee, Microstructural characterization of Al_2O_3–Ni composites prepared by electroless deposition, Surface Coating and Technology 192 (2005) 39–42.

[6] T. Venugopal, K.P. Rao, B.S. Murty, Synthesis of copper–alumina nanocomposite by reactive milling, Material Science and Engineering A 393 (2005) 382–386.

[7] M.F. Amateau, B. Stutzman, J.C. Conway, J. Halloran, Performance of laminated ceramic composite cutting tools, Ceramics International 21 (1995) 317–323.

[8] B.T. Lee, K. Hiraga, Crack propagation and deformation behavior of Al_2O_3–24 vol.% ZrO_2 composite studied by transmission electron microscopy, Journal of Materials Research 9 (1994) 1199–1207.

[9] A.J.S. Herencia, J.S. Moya, A.P. Tomsia, Microstructural design in alumina-alumina/zirconia layered composites, Scripta Materialia 38 (1997) 1–5.

[10] B.T. Lee, K.H. Kim, J.K. Han, Microstructures and material properties of fibrous Al_2O_3–(m-ZrO_2)/t-ZrO_2 composites fabricated by a fibrous monolithic process, Journal of Materials Research 19 (2004) 3234–3241.

[11] R. Bermejo, A.J.S. Herencia, L. Llanes, C. Baudín, High-temperature mechanical behavior of flaw tolerant alumina–zirconia multilayered ceramics, Acta Materialia 55 (2007) 4891–4901.

[12] C.V. Hoy, A. Barda, M. Griffith, J.W. Halloran, Microfabrication of ceramics by co-extrusion, Journal of American Ceramic Society 81 (1998) 152–158.

[13] R.W. Trice, J.W. Halloran, Investigation of the physical and mechanical properties of hot-pressed boron nitride/oxide ceramic composites, Journal of American Ceramic Society 82 (1999) 2563–2565.

[14] B.T. Lee, D.H. Jang, I.C. Kang, C.W. Lee, Relationship between microstructures and material properties of novel fibrous Al_2O_3–(m-ZrO_2)/t-ZrO_2 composites, Journal of American Ceramic Society 88 (2005) 2874–2878.

[15] B.T. Lee, S.K. Sarkar, A.K. Gain, S.J. Yim, H.Y. Song, Core/shell volume effect on the microstructure and mechanical properties of fibrous Al_2O_3–(m-ZrO_2)/t-ZrO_2 composite, Material Science and Engineering A 432 (2006) 317–323.

[16] H. Mills, S. Blackburn, Zirconia toughened alumina by hydro-thermal processing, Journal of European Ceramic Society 20 (2000) 1085–1090.